Journal of Nanoparticle Research **2:** 401–411, 2000.

Electron spins in quantum dots as quantum bits

Daniel Loss[1], Guido Burkard[1] and David P. DiVincenzo[2]
[1]*Department of Physics and Astronomy, University of Basel, Klingelbergstrasse 82, CH-4056 Basel, Switzerland;*
[2]*IBM Research Division, T.J. Watson Research Center, P.O. Box 218, Yorktown Heights, NY 10598, USA*
(Tel.: +41 61 267 3749; Fax: +41 61 267 1349; E-mail: Daniel.Loss@unibas.ch)

Accepted 4 October 2000

Key words: quantum computing, spin, spintronics, spin coherence, quantum dots

Abstract

The creation, coherent manipulation, and measurement of spins in nanostructures open up completely new possibilities for electronics and information processing, among them quantum computing and quantum communication. We review our theoretical proposal for using electron spins in quantum dots as quantum bits, explaining why this scheme satisfies all the essential requirements for quantum computing. We include a discussion of the recent measurements of surprisingly long spin coherence times in semiconductors. Quantum gate mechanisms in laterally and vertically tunnel-coupled quantum dots and methods for single-spin measurements are introduced. We discuss detection and transport of electronic EPR pairs in normal and superconducting systems.

1. Introduction

A computer that processes quantum states instead of conventional classical information is capable of efficiently solving some problems for which there is no efficient classical algorithm [1,2]. Efficiency in this context means that the required computational resources (time, memory) scale polynomially with the size of the problem (input data). The memory of such a quantum computer is usually represented as a collection of quantum two-level systems, named quantum bits, or qubits. The reason why we do not have working quantum computers yet is that it is very hard to find a suitable physical realization of qubits, because the requirements [3,4] for their implementation are extremely demanding. Quantum phase coherence needs to be maintained over a long time compared to the length of an elementary step in the computation, in order to allow for quantum error correction [5]. As a further requirement, it has to be possible to couple pairs of qubits in a controlled manner in order to carry out elementary quantum logic. Moreover, operations on single qubits need to be implemented, and at the end of a computation, the qubits have to be read out by performing a quantum measurement. Finally, the design of the quantum computer should be scalable to a large number of qubits.

On one hand, systems involving trapped atoms [6], cavity QED [7], or nuclear magnetic resonance [8] seem to satisfy all but the scaling requirement from above, and small-scale quantum gate operations with these systems have indeed been demonstrated in experiment. On the other hand, the rapid upscaling of conventional integrated circuits using semiconductor nanotechnology suggests that a similar upscaling might be possible for a solid-state qubit. Several solid-state implementations for quantum computing have been proposed [9–14]. In this paper, we focus on the idea of using electron spins in coupled semiconductor quantum dots as the qubits of a quantum computer [9], and give an overview of the theoretical work that we have carried out in this area. In [9] we have introduced a complete concept of a spin-based quantum computer which has served as a guideline for a number of subsequent

proposals. We devote one section to the discussion of each of the remaining four requirements in the context of quantum dots, viz. coherent qubit, controlled coupling, single-spin operations, and measurement. We then turn to a discussion of quantum communication in terms of electronic Einstein–Podolsky–Rosen (EPR) pairs. We show that such EPR pairs can be transported and detected in transport and noise measurements in electronic nanostructures.

In what follows, quantum dots in semiconductors play an important role and thus some general remarks about these systems are in order. Semiconductor quantum dots are structures in which charge carriers are confined in all three dimensions, their size being of the order of the Fermi wavelength in the host material, typically between 10 nm and 1 μm [15]. The confinement is usually achieved by electrical gating of a two-dimensional electron gas (2DEG), sometimes combined with the application of etching techniques. Precise control of the number of electrons occupying a quantum dot (starting from zero) has been achieved in GaAs heterostructures [16]. The electronic spectrum of typical quantum dots can vary strongly when an external magnetic field is applied [15–17], since the magnetic length corresponding to typical laboratory fields ($B \approx 1\,\mathrm{T}$) is comparable to typical dot sizes. In coupled quantum dots, Coulomb blockade effects [18] and magnetization [19] have been observed as well as the formation of a delocalized 'molecular state' [20].

2. Spin coherence in semiconductors

Recent magneto-optical experiments have shown surprisingly long spin coherence times in doped GaAs bulk semiconductors [21]. At zero field and $T = 5\,\mathrm{K}$, the transverse spin lifetime (coherence time) T_2^* can exceed 100 ns. Since this number still includes inhomogeneous broadening, e.g. due to g-factor variations in the material, it represents only a lower bound on the transverse lifetime of a *single* spin, $T_2 \geq T_2^*$, which is relevant for using spins as qubits.

In [21] the spin coherence time was measured using time-resolved Faraday rotation. This method involves optically generating (pumping) a spin polarization perpendicular to the externally applied field using circularly polarized light (propagating perpendicularly to the applied field). The time-dependent magnetization of the electrons precessing in the external field is then $M(t) = M(0)\cos(g\mu_B Bt/\hbar)\exp(-t/T_2^*)$, where the cosine describes the coherent precession of the spins about the external field B (with μ_B the Bohr magneton and g the effective g-factor of the semiconductor), and the exponential represents the loss of coherence on a time scale T_2^*. The magnetization $M(t)$ (and thus T_2^*) can be mapped out by probing the spin magnetization of the semiconductor after a delay t, ranging from a few ps to ns. Here, one makes use of the so-called Faraday rotation: the polarization of a linearly polarized laser pulse arriving at the sample at time t is rotated by an angle which is proportional to $M(t)$. This pump-probe procedure is then repeated for an entire series of delay times t, finally revealing the spin precession $M(t)$ and the decoherence time T_2^*. Using the same method, spin lifetimes in semiconductor quantum dots have been measured [22]. The relatively small T_2^* (a few ns at zero field) which have been seen in these experiments probably originate from a large inhomogeneous broadening due to a strong variation of g-factors. Thus, the fact that many coherent oscillations were observed in these recent spin measurements by the Awschalom group provides strong experimental support to the idea to use electron spin as qubits.

3. Quantum gate operations with coupled quantum dots

In addition to phase-coherent qubits, we are also interested in a mechanism that couples pairs of qubits. For electron spins in coupled quantum dots, the required mechanism is provided by the combined action of the Coulomb interaction and the Pauli exclusion principle. At zero magnetic field, the ground state of two coupled electrons is a spin singlet, whereas the first excited state in the presence of strong Coulomb repulsion is usually a triplet. The remaining spectrum is separated from these two states by a gap which is either defined by the Coulomb repulsion or the single particle confinement. The low-energy physics of such a system can then be described by the Heisenberg spin Hamiltonian

$$H_s(t) = J(t)\,\mathbf{S}_1 \cdot \mathbf{S}_2, \tag{1}$$

where $J(t)$ is the exchange coupling between the two spins $\mathbf{S}_1$ and $\mathbf{S}_2$, i.e. the energy difference between the singlet and triplet states. If the exchange coupling is pulsed such that $\int dt\, J(t)/\hbar = J_0\tau_s/\hbar = \pi \pmod{2\pi}$, the associated unitary time evolution $U(t) = T\exp(i\int_0^t H_s(\tau)\,d\tau/\hbar)$ corresponds to the 'swap' operator U_{sw} which simply exchanges the

quantum states of qubit 1 and 2 [9]. Furthermore, the quantum XOR can be obtained by applying the sequence [9]

$$U_{\mathrm{XOR}} = e^{i(\pi/2)S_1^z} e^{-i(\pi/2)S_2^z} U_{\mathrm{sw}}^{1/2} e^{i\pi S_1^z} U_{\mathrm{sw}}^{1/2}, \tag{2}$$

i.e. a combination of 'square-root of swap' $U_{\mathrm{sw}}^{1/2}$ and single-qubit rotations $\exp(i\pi S_i^z)$. Since U_{XOR} (combined with single-qubit rotations) is proven to be a universal quantum gate [23], it can be used to assemble any quantum algorithm. The study of universal quantum computation in coupled quantum dots is thus essentially reduced to the study of the *exchange mechanism* and how the exchange coupling $J(t)$ can be controlled experimentally. Note that the switchable coupling mechanism described below need not be restricted to quantum dots: the same principle can be applied to other systems, e.g. coupled atoms in a Bravais lattice, supramolecular structures, or overlapping shallow donors in semiconductors.

3.1. Laterally coupled quantum dots

We first consider a system of two laterally coupled quantum dots containing one (conduction band) electron each [24]. It is essential that the electrons are allowed to tunnel between the dots, introducing correlations between the spins via the charge (orbital) degrees of freedom. We model the coupled system with the Hamiltonian $H = \sum_{i=1,2} h_i + C + H_{\mathrm{Z}} = H_{\mathrm{orb}} + H_{\mathrm{Z}}$, where

$$h_i = \frac{1}{2m}\left(\mathbf{p}_i - \frac{e}{c}\mathbf{A}(\mathbf{r}_i)\right)^2 + V(\mathbf{r}_i),$$
$$C = \frac{e^2}{\kappa\,|\mathbf{r}_1 - \mathbf{r}_2|}. \tag{3}$$

Here, h_i describes the single-electron dynamics in the 2DEG confined to the xy-plane, with m being the electron band mass. We allow for a magnetic field $\mathbf{B} = (0, 0, B)$ applied along the z-axis and which couples to the electron charge via the vector potential $\mathbf{A}(\mathbf{r}) = B/2(-y, x, 0)$, and to the spin via a Zeeman coupling term H_{Z}. The coupling of the dots (which includes tunneling) is modeled by a quartic potential, $V(x, y) = m\omega_0^2\left((x^2 - a^2)^2/(4a^2) + y^2\right)/2$, which separates into two harmonic wells of frequency ω_0, one for each dot, in the limit $2a \gg 2a_{\mathrm{B}}$, where a is half the distance between the centers of the dots, and $a_{\mathrm{B}} = \sqrt{\hbar/m\omega_0}$ is the effective Bohr radius of a dot. This choice for the potential is motivated by the experimental fact [16] that the low-energy spectrum of single dots is well described by a parabolic confinement potential. The (bare) Coulomb interaction between the two electrons is described by C where κ denotes the dielectric constant of the semiconductor. The screening length λ in almost depleted regions like few-electron quantum dots can be expected to be much larger than the bulk 2DEG screening length (which is about 40 nm in GaAs). Therefore, λ is large compared to the size of the coupled system, $\lambda \gg 2a \approx 40$ nm for small dots, and we will consider the limit of unscreened Coulomb interaction ($\lambda/a \gg 1$).

At sufficiently low temperatures $kT \ll \hbar\omega_0$ we are allowed to restrict our analysis to the two lowest orbital eigenstates of H_{orb}, one of which is symmetric (spin singlet) and the other one antisymmetric (spin triplet). In this reduced (four-dimensional) Hilbert space, H_{orb} can be replaced by the effective Heisenberg spin Hamiltonian Eq. (1), the exchange energy $J = \epsilon_{\mathrm{t}} - \epsilon_{\mathrm{s}}$ being the difference between the triplet and singlet energy. Rather than solving this model in an analytically closed form, we make use of the analogy between atoms and quantum dots (artificial atoms), providing us with a powerful set of variational methods from molecular physics for calculating ϵ_{t} and ϵ_{s}. Using the Heitler–London approximation we find [24],

$$J = \frac{\hbar\omega_0}{\sinh\left(2d^2(2b - 1/b)\right)}\left[\frac{3}{4b}\left(1 + bd^2\right) + c\sqrt{b} \times \left(e^{-bd^2}\mathrm{I}_0(bd^2) - e^{d^2(b-1/b)}\mathrm{I}_0(d^2(b - 1/b))\right)\right], \tag{4}$$

where we introduce the dimensionless distance $d = a/a_{\mathrm{B}}$ and the magnetic compression factor $b = B/B_0 = \sqrt{1 + \omega_{\mathrm{L}}^2/\omega_0^2}$, where $\omega_{\mathrm{L}} = eB/2mc$ is the Larmor frequency. The zeroth order Bessel function is denoted by I_0. The terms in Eq. (4) proportional to the parameter $c = \sqrt{\pi/2}(e^2/\kappa a_{\mathrm{B}})/\hbar\omega_0$ are due to the Coulomb interaction C, where the exchange term enters with a minus sign. The first term in Eq. (4) comes from the confinement potential. Note that typically $|J/\hbar\omega_0| \ll 1$, making the exclusive use of ground-state single-dot orbitals in the Heitler–London ansatz a self-consistent procedure. The exchange J is plotted as a function of B and d in Figure 1. We observe that $J > 0$ for $B = 0$, which must be the case for a two-particle

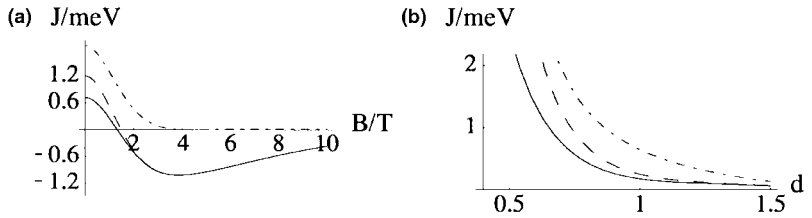

Figure 1. The exchange coupling J (full line) for GaAs quantum dots with confinement $\hbar\omega = 3$ meV and $c = 2.42$. For comparison we plot the usual short-range Hubbard result $J = 4t^2/U$ (dashed–dotted line) and the extended Hubbard result [24] $J = 4t^2/U + V$. In (a), J is plotted as a function of the magnetic field B at fixed inter-dot distance ($d = a/a_B = 0.7$), and in (b) as a function of the inter-dot distance $d = a/a_B$ at zero field ($B = 0$).

system that is time-reversal invariant. The most remarkable feature of $J(B)$, however, is the change of sign from positive to negative, which occurs at some finite B over a wide range of parameters c and a. The transition from antiferromagnetic ($J > 0$) to ferromagnetic ($J < 0$) spin–spin coupling with increasing magnetic field is caused by the long-range Coulomb interaction, in particular by the negative exchange term. Large magnetic fields ($b \gg 1$) compress the electron orbitals and thereby lead to the exponential decrease of J contained in the $1/\sinh$ prefactor in Eq. (4). Similarly, the orbital overlap between the two dots (and thus J) decays exponentially for $d \gg 1$. Note, however, that this exponential suppression is partly compensated by the exponentially growing exchange term $\propto \exp(2d^2(b-1/b))$. As a result, J decays exponentially as $\exp(-2d^2b)$ for large b or d. Thus, J can be tuned through zero and then exponentially suppressed to zero by a magnetic field in a very efficient way (exponential switching is highly desirable to minimize gate errors). This sign reversal of J is due to the long-range Coulomb forces and is not contained in the standard Hubbard approximation which takes only short-range interactions into account, and where one finds $J = 4t^2/U > 0$ in the limit $t/U \ll 1$ (see Figure 1). By working around the magnetic field where J vanishes the exchange interaction can be pulsed on, even without changing the tunneling barrier between the dots, by an application of a local magnetic field.

Qualitatively similar results are obtained [24] when we refine above Heitler–London result by taking into account higher levels and double occupancy of the dots (requiring a molecular orbit approach). Finally, we note that a spin coupling can also be achieved on a long distance scale by using a cavity-QED scheme [25] or superconducting leads to which the quantum dots are attached [26].

3.2. Vertically coupled quantum dots

Motivated by the experimental progress in the fabrication of both multilayer self-assembled quantum dots (SAD) [27] as well as etched mesa heterostructures [28], both with vertical coupling, we have investigated the exchange coupling in vertically tunnel-coupled quantum dots [29]. The same methods as for laterally coupled quantum dots were used. However, the two-dimensional Hamiltonian Eq. (3) had to be replaced by a three-dimensional one, taking into account the confinement $V = V_l + V_v$ in all three dimensions. The vertical confinement V_v is assumed to have the form of a double-well, as for the lateral confinement in the two-dimensional case with curvature ω_z at $z = \pm a$, as shown in Figure 2(b). Here, the lateral confinement potential V_l is a simple harmonic well. We have, however, included the possibility that the two quantum dots have different lateral sizes $a_{B\pm} = \sqrt{h/m\alpha_{0\pm}\omega_z}$, leading to interesting new effects when external fields are applied (see below). As a consequence of being three-dimensional, the exchange interaction in vertically coupled quantum dots is sensitive to magnetic and electric fields in different directions. Here, we summarize our results [29] for in-plane ($\parallel$) and perpendicular ($\perp$) fields (see Figure 2(a)): (1) An in-plane magnetic field has essentially the same effect as a perpendicular field in laterally coupled dots; it suppresses the exchange J exponentially. (2) Perpendicular magnetic fields reduce the exchange coupling between identical dots only very weakly. However, if two dots of different sizes are coupled, then we expect a non-monotonic behavior of J as a function of B. Increasing B from zero, the exchange first increases until $B = 2mc\omega_z\alpha_{0+}/e$, when both electronic orbitals are magnetically compressed to approximately the same size; then, J decreases weakly, as in the case of identical dots. (3) Perpendicular electric

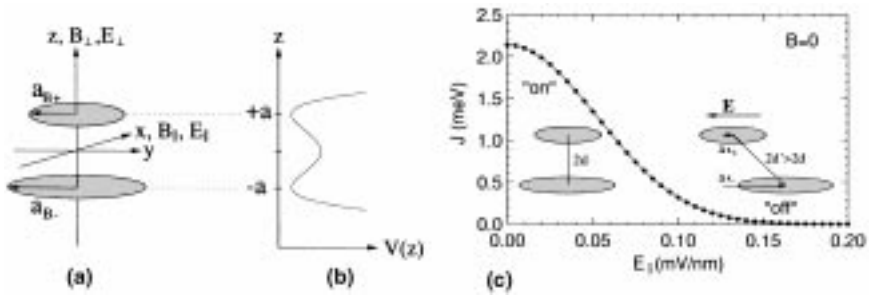

Figure 2. (a) Sketch of the vertically coupled double quantum-dot system. The two dots may have different lateral diameters, a_{B+} and a_{B-}. We consider magnetic and electric fields applied either in-plane ($B_\parallel$, $E_\parallel$) or perpendicularly ($B_\perp$, $E_\perp$). (b) The model potential for the vertical confinement is a double-well, which is obtained by combining two harmonic wells with frequency ω_z at $z = \pm a$. (c) Switching of the spin–spin coupling between dots of different size by means of an in-plane electric field $E_\parallel$ ($B = 0$). The exchange coupling is switched 'on' at $E = 0$ (see text). We have chosen $\hbar\omega_z = 7\,\mathrm{meV}$, $d = 1$, $\alpha_{0+} = 1/2$ and $\alpha_{0-} = 1/4$. For these parameters, $E_0 = \hbar\omega_z/ea_B = 0.56\,\mathrm{mV/nm}$ and $A = (\alpha_{0+}^2 - \alpha_{0-}^2)/2\alpha_{0+}^2\alpha_{0-}^2 = 6$. The exchange coupling J decreases exponentially on the scale $E_0/2A = 47\,\mathrm{mV/\mu m}$ for the electric field.

fields simply detune the single-dot levels, therefore reducing the exchange coupling. This effect can also be found for laterally coupled dots. (4) In-plane electric fields $E_\parallel$ have a very interesting effect for coupled dots of different size, see Figure 2(c). The larger of the two dots is shifted by Δx_-, whereas the smaller dot is shifted by $\Delta x_+ < \Delta x_-$, where $\Delta x_\pm = E_\parallel/E_0\alpha_{0\pm}^2$ and $E_0 = \hbar\omega_z/ea_B$. Therefore, the mean distance between the electrons in the two dots grows as $d' = \sqrt{d^2 + A^2(E_\parallel/E_0)^2}$, where $A = (\alpha_{0+}^2 - \alpha_{0-}^2)/2\alpha_{0+}^2\alpha_{0-}^2$. The exchange coupling J, Eq. (4), being exponentially sensitive to the inter-dot distance d', decreases thus exponentially, $J \approx S^2 \approx \exp[-2A^2(E_\parallel/E_0)^2]$. With this effect we have found another exponential switching mechanism for quantum gate operation.

4. Single-spin rotations

The theoretical requirement for the single-spin rotations for a spin-1/2 qubit is the following: it must be possible to subject a specified qubit to a (real or effective) magnetic field of specified direction and strength. We have presented various ideas of how to achieve this previously [9,24]: by the application of real, localized magnetic fields using a scanned magnetic particle or nanoscale electric currents; using a magnetized dot or magnetized barrier material that the electron can be inserted in and out of by electric gating; or by the use of g-factor-modulated materials [3,4]. We would like to sketch the analysis of the last idea here.

Due to spin-orbit coupling, the Landé g-factor in bulk semiconductor materials differs from the free-electron value $g_0 = 2.0023$ and ranges from large negative to large positive numbers for various materials. In confined structures such as quantum wells, wires, and dots, the g-factor is modified with respect to the bulk material and sensitive to an external bias voltage [30]. We have studied the simpler case of a layered structure in which the effective g-factor of electrons is varied by electrically shifting their equilibrium position from one layer (with g-factor g_1) to another (with another g-factor $g_2 \neq g_1$). For simplicity, we use the bulk g-factors of the layer materials, an approximation which becomes increasingly inaccurate as the layers become thinner [31].

We consider a quantum well (e.g. AlGaAs–GaAs–AlGaAs), in which some fraction y of the Ga atoms are replaced by In atoms in the upper half of the heterostructure (we have used $y = 0.1$). The sequence of layers in the heterostructure is then $Ga_{1-x}Al_xAs$–GaAs–$Ga_{1-y}In_yAs$–$Ga_{1-x}Al_xAs$, where x denotes the Al content in the barriers (typically around 30%). Changing the vertical position of the electrons in the quantum well via top or back gates permits control of the effective g-factor for the corresponding electrons. If the electron is mostly in a pure GaAs environment, then its effective g-factor will be around the GaAs bulk value ($g_{GaAs} = -0.44$) whereas if the electron is in the InGaAs region, the g-factor will be somewhere between the GaAs and the InAs values ($g_{InAs} = -15$). We have numerically analyzed the one-dimensional problem of a single electron in such a structure (screening effects are neglected since we are interested in

isolated electrons located in quantum dots),

$$\left[-\frac{d}{dz}\frac{\hbar^2}{2m(z)}\frac{d}{dz}+V(z)\right]\Psi(z)=E\Psi(z), \qquad (5)$$

with a spatially varying effective mass $m(z)$ by discretizing it in real space and subsequently performing exact diagonalization [4]. The potential $V(z)$ describes the quantum well (conduction band offset $\Delta E_c = 270\,\mathrm{meV}$) and the electric field E in growth direction. For the effective masses and g-factors of the various layers we have linearly interpolated between the GaAs, AlAs, and InAs values. The resulting effective g-factor was calculated by averaging the g-factor over the electronic ground-state wavefunction, $g_{\mathrm{eff}} = \int dz\, g(z)|\Psi(z)|^2$. We find that at moderate electric fields, g_{eff} interpolates roughly between the GaAs and $Ga_{1-y}In_yAs$ g-factors. If the electric energy $eEw_B = eU_B$ becomes larger than the barrier ΔE_c, we observe a vertical deconfinement of the electrons. The electric field required for a substantial change in g_{eff} is of the order of $10\,\mathrm{mV/nm}$, corresponding to a voltage of 100 mV, which is about one order of magnitude smaller than the band gap (1.5 eV for GaAs at $T = 0$). Since for the above materials and parameters the Zeeman energy is about 100 times smaller than the typical kinetic energy, we find no noticeable deviation from the linear relation $\Delta E(B) \simeq g_{\mathrm{eff}}\mu_B B$ which might arise due to the Zeeman coupling.

The described quantum well can host an array of electrostatically defined quantum dots, containing a single excess electron (and thus a single spin 1/2) each. In order to carry out a single-qubit operation on one of the spins, the whole system is placed into a homogeneous magnetic field. By changing the voltage at the electric gate on top of a single quantum dot, the effective g-factor g_{eff} for the spin in this quantum dot can be changed by about $\Delta g_{\mathrm{eff}} \approx 1$ with respect to the g-factor of all remaining spins. This leads to a relative rotation about the direction of $\mathbf{B}$ by an angle of roughly $\phi = \Delta g_{\mathrm{eff}}\mu_B B\tau/2\hbar$. The typical switching time τ for a $\phi = \pi/2$ rotation using a field of 1 T is then approximately $\tau \approx 2\phi\hbar/\Delta g_{\mathrm{eff}}\mu_B B \approx 30\,\mathrm{ps}$. Controlling the top gate at $\tau^{-1} \approx 30\,\mathrm{GHz}$ seems very challenging; we emphasize however that the single-qubit operation can be done much more slowly (a lower limit is provided by the spin dephasing time). The switching can be slowed down either by choosing a smaller Δg_{eff} or by replacing ϕ by $\phi + 2\pi n$ where n is an integer. Once we have the possibility to generate different Zeeman splittings for each qubit (either by an inhomogeneous magnetic field or inhomogeneous g-factors) we can perform the switching also by ESR methods [24], where we apply in addition a homogeneous but time-dependent field B_{ac} with an oscillation frequency that matches the Zeeman splitting energy of the particular qubit one wants to address.

5. Single-spin measurements

Measurements of the Faraday rotation (cf. Section 2) originating from a single pair of coupled electrons would allow us to distinguish between spin singlet and triplet [29]. If the system is in the singlet state ($S = 0$, no magnetic moment) there is no Faraday rotation, whereas in the triplet state ($S = 1$) the polarization of linearly polarized light is rotated slightly due to the presence of a finite magnetic moment. Such individual singlet and triplet states in a double dot can also be detected (through their charge) in transport measurements via Aharonov–Bohm oscillations in the cotunneling current and/or current correlations [3,32,33] (see below).

Above schemes even allow the measurement of a single spin 1/2, provided that it is possible to perform one two-qubit gate operation (see Section 3) and a subsequent single-qubit gate (see Section 4). Explicitly, such a single-spin measurement of the electron is performed as follows [29]. We are given an arbitrary spin 1/2 state $|\alpha\rangle$ in quantum dot 1. For simplicity, we assume that $|\alpha\rangle$ is one of the basis states, $|\alpha\rangle = |\uparrow\rangle$ or $|\alpha\rangle = |\downarrow\rangle$; the generalization to a superposition of the basis states is straightforward. The spin in quantum dot 2 is prepared in the state $|\uparrow\rangle$. Then, a $U_{\mathrm{sw}}^{1/2}$ gate is performed (cf. Section 3). In the case $|\alpha\rangle = |\uparrow\rangle$, nothing happens, i.e. the spins remain in the state $|\uparrow\uparrow\rangle$, whereas if $|\alpha\rangle = |\downarrow\rangle$, we obtain the entangled state $(|\downarrow\uparrow\rangle + i|\uparrow\downarrow\rangle)/\sqrt{2}$ (up to a phase factor which can be ignored). Finally, we apply a local Zeeman term, $g\mu_B B S_z^1$, acting parallel to the z-axis at quantum dot 1 during the time interval τ_B, such that $\int_0^{\tau_B}(g\mu_B B)(t)\,dt = \pi/2$. The resulting state is (again up to unimportant phase factors) the triplet state $|\uparrow\uparrow\rangle$ in the case where $|\alpha\rangle = |\uparrow\rangle$, whereas we obtain the singlet state $(|\uparrow\downarrow\rangle - |\downarrow\uparrow\rangle)/\sqrt{2}$ in the case $|\alpha\rangle = |\downarrow\rangle$. In other words, such a procedure maps the triplet $|\uparrow\uparrow\rangle$ into itself and the state $|\downarrow\uparrow\rangle$ into the singlet (similarly, the same gate operations map $|\downarrow\downarrow\rangle$ into itself, while $|\uparrow\downarrow\rangle$ is mapped into the triplet $(|\uparrow\downarrow\rangle + |\downarrow\uparrow\rangle)/\sqrt{2}$, again up to phase factors). Finally, measuring the total magnetic moment of the double dot system then reveals which

of the two spin states in dot 1, $|\uparrow\rangle$ or $|\downarrow\rangle$, was realized initially. Note that it is also possible that a *single* spin 1/2 will be directly measured via Faraday rotation, or by making use of spin-selective tunneling devices with subsequent charge detection [9].

6. Quantum communication with electrons: detection of entanglement [3,32,33,45]

The availability of pairwise entangled qubits – EPR pairs [35] – is a necessary prerequisite in quantum communication [34]. The prime example of an EPR pair considered here is the singlet state formed by two electron spins, its main feature being its non-locality. If we separate the two electrons in real space, their total spin state can still remain entangled. Such non-locality gives rise to striking phenomena such as violations of Bell inequalities and quantum teleportation and has been investigated for photons [36,37], but not yet for *massive* particles such as electrons, let alone in a solid-state environment. This is so because it is difficult to first produce and to second detect entanglement of electrons in a controlled way. In this section we describe several experimental setups by which the entanglement of electrons (once produced as e.g. described in the previous section) can be detected via their charge in transport and noise measurements [26,32,33].

6.1. Bunching and antibunching of EPR pairs

We consider the setup shown in Figure 3. Here, the entangler is assumed to be a device by which we can generate (or detect) entangled electron states, a specific realization being the double-dot system discussed in previous sections. The presence of a beam splitter ensures that the electrons leaving the entangler have a finite amplitude to be interchanged (with or without mutual interaction). The quantity of interest is then the current–current correlations (noise) measured in leads 3 and/or 4.

It is well-known [38] that particles with symmetric wave functions show bunching behavior [39] in the noise, whereas particles with antisymmetric wave functions show antibunching behavior. The latter situation is the one considered so far for electrons in the normal state both in theory [40,41] and in experiments [42]. However, since the noise is produced by the charge degrees of freedom we can expect [3] that in the absence of spin scattering processes the noise is sensitive to the

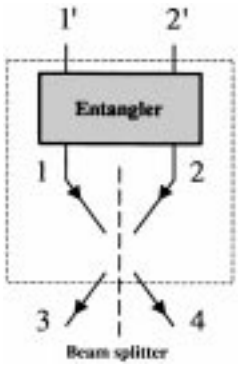

Figure 3. Uncorrelated electrons are fed into the entangler through the Fermi leads $1'$ and $2'$. The entangler is a device (see text) that produces pairs of electrons in the entangled spin singlet or one of the spin triplets and injects one of the electrons into lead 1 and the other into lead 2. In the outgoing leads, for singlets we get bunching due to their orbital symmetry, whereas for triplets we get antibunching due to their orbital antisymmetry.

symmetry of only the *orbital part* of the wave function. On the other hand, since the spin singlet of two electrons is uniquely associated with a symmetric orbital wave-function, and the three triplets with an antisymmetric one we have thus a means to distinguish singlets from triplets through a bunching or antibunching signature. Below we verify this expectation explicitly, by extending the standard scattering matrix approach [40,41] to a situation with entanglement.

The operator for the current carried by electrons with spin σ in lead α of a multiterminal conductor can be written as [32,40]

$$I_{\alpha\sigma}(t) = \frac{e}{h\nu}\sum_{E,E'}[a^{\dagger}_{\alpha\sigma}(E)a_{\alpha\sigma}(E') - b^{\dagger}_{\alpha\sigma}(E)b_{\alpha\sigma}(E')]e^{i(E-E')t/\hbar}, \tag{6}$$

where $a^{\dagger}_{\alpha\sigma}(E)$ creates an incoming electron in lead α with spin σ and energy E, and the operators $b_{\alpha\sigma}$ for the outgoing electrons are related to the operators $a_{\alpha\sigma}$ for the incident electrons via the scattering matrix, $s_{\alpha\beta}$, $b_{\alpha\sigma}(E) = \sum_{\beta} s_{\alpha\beta}a_{\beta\sigma}(E)$. We will assume that the scattering matrix is spin- and energy-independent. Note that since we are dealing with discrete energy states here, we normalize the operators $a_{\alpha\sigma}(E)$ such that $\{a_{\alpha\sigma}(E), a_{\beta\sigma'}(E')^{\dagger}\} = \delta_{\sigma\sigma'}\delta_{\alpha\beta}\delta_{E,E'}/\nu$, where $\delta_{E,E'}$ is the Kronecker symbol, and ν the density of states. We assume that each lead consists of only a single quantum

channel. We then obtain

$$I_{\alpha\sigma}(t) = \frac{e}{h\nu}\sum_{E,E'}\sum_{\beta\gamma} a^{\dagger}_{\beta\sigma}(E)A^{\alpha}_{\beta\gamma}a_{\gamma\sigma}(E')e^{i(E-E')t/\hbar},$$
$$A^{\alpha}_{\beta\gamma} = \delta_{\alpha\beta}\delta_{\alpha\gamma} - s^{*}_{\alpha\beta}s_{\alpha\gamma}. \quad (7)$$

We restrict ourselves here to unpolarized currents, $I_\alpha = \sum_\sigma I_{\alpha\sigma}$. The spectral density of the current fluctuations (noise) $\delta I_\alpha = I_\alpha - \langle I_\alpha\rangle$ between the leads α and β are defined as

$$S_{\alpha\beta}(\omega) = \lim_{T\to\infty}\frac{h\nu}{T}\int_0^T dt\ e^{i\omega t}\langle\Psi|\delta I_\alpha(t)\delta I_\beta(0)|\Psi\rangle, \quad (8)$$

where the state $|\Psi\rangle$ is some arbitrary state to be specified below. Inserting the expression for the currents Eq. (7) into this definition, we obtain for the zero frequency correlations

$$S_{\alpha\beta} = \frac{e^2}{h\nu}\sum_{\gamma\delta\epsilon\zeta} A^{\alpha}_{\gamma\delta}A^{\beta}_{\epsilon\zeta} \times \sum_{E,E',\sigma\sigma'}\Big[\langle\Psi|a^{\dagger}_{\gamma\sigma}(E)a_{\delta\sigma}(E)a^{\dagger}_{\epsilon\sigma'}(E')a_{\zeta\sigma'}(E')|\Psi\rangle - \langle\Psi|a^{\dagger}_{\gamma\sigma}(E)a_{\delta\sigma}(E)|\Psi\rangle\langle\Psi|a^{\dagger}_{\epsilon\sigma'}(E')a_{\zeta\sigma'}(E')|\Psi\rangle\Big]. \quad (9)$$

We note that since $|\Psi\rangle$ in general does not describe a Fermi liquid state, it is not possible to apply Wick's theorem.

6.2. Noise for entangled states

We will now investigate the noise correlations for scattering with the entangled incident state $|\Psi\rangle = |\pm\rangle$, where

$$|\pm\rangle = \tfrac{1}{\sqrt{2}}\left(a^{\dagger}_{2\downarrow}(\epsilon_2)a^{\dagger}_{1\uparrow}(\epsilon_1) \pm a^{\dagger}_{2\uparrow}(\epsilon_2)a^{\dagger}_{1\downarrow}(\epsilon_1)\right)|0\rangle.$$

The state $|-\rangle$ is the spin singlet, $|S\rangle$, while $|+\rangle$ denotes one of the spin triplets $|T_{0,\pm}\rangle$; in the following we will present a calculation of the noise for $|+\rangle = |T_0\rangle$, i.e. the triplet with $m_z = 0$.

Using $|\pm\rangle$ for $|\Psi\rangle$, we get $\langle\pm|\delta I_\alpha\delta I_\beta|\pm\rangle = \langle\uparrow\downarrow|\delta I_\alpha\delta I_\beta|\uparrow\downarrow\rangle \pm \langle\uparrow\downarrow|\delta I_\alpha\delta I_\beta|\downarrow\uparrow\rangle$, where the upper (lower) sign of the exchange term refers to triplet (singlet). After some straightforward manipulations, we obtain the following result for the correlations between the leads α and β,

$$S_{\alpha\beta} = \frac{e^2}{h\nu}\left[\sum_{\gamma\delta}{}' A^{\alpha}_{\gamma\delta}A^{\beta}_{\delta\gamma} \mp \delta_{\epsilon_1,\epsilon_2}(A^{\alpha}_{12}A^{\beta}_{21} + A^{\alpha}_{21}A^{\beta}_{12})\right],$$

where $\sum'_{\gamma\delta}$ denotes the sum over $\gamma = 1, 2$ and all $\delta \neq \gamma$, and where again the upper (lower) sign refers to triplets (singlets).

We apply above formula now to the set-up shown in Figure 3 involving four leads, described by the scattering matrix elements, $s_{31} = s_{42} = r$, and $s_{41} = s_{32} = t$, where r and t denote the reflection and transmission amplitudes at the beam splitter, respectively, and with no backscattering, $s_{12} = s_{34} = s_{\alpha\alpha} = 0$. The unitarity of the s-matrix implies $|r|^2 + |t|^2 = 1$, and $\mathrm{Re}[r^* t] = 0$. Using above relations, we obtain finally*,

$$S_{33} = S_{44} = -S_{34} = 2\frac{e^2}{h\nu}T(1-T)(1 \mp \delta_{\epsilon_1,\epsilon_2}), \quad (10)$$

where $T = |t|^2$ is the probability for transmission through the beam splitter. The calculation for the remaining two triplet states $|+\rangle = |T_\pm\rangle = |\uparrow\uparrow\rangle, |\downarrow\downarrow\rangle$ yields the same result Eq. (10) (upper sign). Note that the total current $\delta I_3 + \delta I_4$ does note fluctuate, i.e. $S_{33} + S_{44} + 2S_{34} = 0$, since we have excluded backscattering. For the average current in lead α we obtain $|\langle I_\alpha\rangle| = e/h\nu$, with no difference between singlets and triplets. Then, the Fano factor $F = S_{\alpha\alpha}/|\langle I_\alpha\rangle|$ takes the following form:

$$F = 2eT(1-T)(1 \mp \delta_{\epsilon_1,\epsilon_2}), \quad (11)$$

and correspondingly for the cross correlations. This result confirms our expectation stated in the introduction: if two electrons with the same energies, $\epsilon_1 = \epsilon_2$, in the singlet state $|S\rangle = |-\rangle$ are injected into the leads 1 and 2, then the zero frequency noise is *enhanced* by a factor of two, $F = 4eT(1-T)$, compared to the shot noise of uncorrelated particles, $F = 2eT(1-T)$. This enhancement of noise is due to *bunching* of electrons in the outgoing leads, caused by the symmetric orbital wavefunction of the spin singlet $|S\rangle$. On the other hand, the triplet states $|+\rangle = |T_{0,\pm}\rangle$ exhibit an *antibunching* effect, leading to a complete suppression of the zero-frequency noise in Eq. (10), $S_{\alpha\alpha} = 0$. The noise enhancement for the singlet $|S\rangle$ is a unique signature for entanglement (there exists no unentangled state with the same symmetry), therefore entanglement can be observed by measuring the noise power of a mesoscopic conductor. The triplets can be further distinguished from each other if we can measure the spin of the two electrons in the outgoing leads, or if we

*For finite frequencies, we obtain the noise power $S_{\alpha\alpha}(\omega) = (e^2/h\nu)[(1-\delta_{\omega,0}) + T(1-T)(2\delta_{\omega,0} \mp \delta_{\omega_1(\epsilon_1-\epsilon_2)/\hbar}) \mp \delta_{\omega_1(\epsilon_2-\epsilon_1)/\hbar}]$.

insert spin-selective tunneling devices [43] into leads 3, 4 which would filter a certain spin polarization.

We emphasize that above results remain unchanged if we consider states $|\pm\rangle$ which are created above a Fermi sea. We have shown [3] that the entanglement of two electrons propagating in a Fermi sea gets reduced by the quasiparticle weight z_F (for each lead one factor) due to the presence of interacting electrons. In the metallic regime, z_F assumes typically some finite value†, and thus as long as spin scattering processes are small the above description for non-interacting electrons remains valid.

6.3. *Noise induced by spin currents [32,45,46]*

In this subsection we discuss the current noise induced by the spin transport in a two-terminal conductor attached to Fermi leads with spin-dependent chemical potentials μ_σ. It is clear that for a stationary situation a spin reservoir (at chemical potential μ_σ) is needed. In particular, it is not sufficient to just apply a magnetic field gradient along the sample to create a stationary spin current, since an inhomogeneous field simply leads to an inhomogeneous magnetization build-up and after some short relaxation time an initial spin current vanishes again. To avoid such a saturation of the spin current one could make use of an oscillating (in time) magnetic field gradient, with a frequency which is larger than the spin relaxation frequency but still small enough so that the zero-frequency limit considered above remains applicable. For the present purpose we simply assume that it is possible to induce a spin-dependent chemical potential difference leading to a stationary spin current (but not necessarily to a charge current). From Eq. (7) we immediately obtain $\langle I_\sigma\rangle = e/hT\,\Delta\mu_\sigma$, where we have introduced the difference of chemical potentials $\Delta\mu_\sigma = \mu_{1\sigma} - \mu_{2\sigma}$ for each spin orientation σ. Then, applying Wick's theorem to Eq. (9) we obtain the noise power $S = e^2/hT(1-T)(|\Delta\mu_\uparrow| + |\Delta\mu_\downarrow|)$. Thus, the contribution of two spin subsystems to the noise is independent, as it should be if there is no spin interaction. Therefore, we can rewrite above expression as $S = e(1-T)(|\langle I_\uparrow\rangle| + |\langle I_\downarrow\rangle|)$. In particular, when $\Delta\mu_\uparrow = \Delta\mu_\downarrow$ we obtain the usual result [45] $S = e(1-T)|I_c|$ for the shot noise induced by the charge current $I_c \equiv \langle I_\uparrow\rangle + \langle I_\downarrow\rangle$. On the other hand, we can consider the situation where $\Delta\mu_\uparrow = -\Delta\mu_\downarrow$, and thus there is no charge current through the conductor, $I_c = 0$. Still, there is a non-vanishing spin current $I_s \equiv \langle I_\uparrow\rangle - \langle I_\downarrow\rangle$, and according to the above result one can observe the current noise $S = e(1-T)|I_s|$ induced by spin transport only.

† For instance, in metals such as bulk Cu the quasiparticle weight becomes within RPA approximation $z_F = 0.77$, while for a GaAs 2DEG we find [3] (also within RPA) $z_F = 1 - r_s(1/2 + 1/\pi) = 0.66$ for the GaAs interaction parameter $r_s = 0.61$.

6.4. *Spin-dependent current through a double-dot [33]*

We turn now to a further scenario where entanglement can be measured in the current [33]. A double-dot system which is weakly coupled to an ingoing (1) and an outgoing (2) lead held at chemical potentials $\mu_{1(2)}$, but where now an electron coming from lead 1(2) has the option to tunnel into *both* dots 1 and 2 with amplitude Γ. In contrast to previous studies the double-dot is put in parallel instead of in series between the two leads. This results in a closed loop, and applying a magnetic field, an Aharonov–Bohm phase φ will be acquired by an electron traversing the double-dot. Note that the double-dot (containing two entangled electrons with the singlet being their ground state) can be viewed as an artificial H_2 molecule (this should be carefully distinguished from the singlet in a single dot like an He-atom, which cannot be used for the present purpose because the two electrons are not separated in space). In the Coulomb blockade regime where the electron number on the dots is quantized and kept fixed we find that due to cotunneling the current traversing the double-dot becomes

$$I = e\pi\nu^2\Gamma^4\frac{\mu_1 - \mu_2}{\mu_1\mu_2}(2 \pm \cos\varphi), \tag{12}$$

where the upper (lower) sign refers to triplet (singlet) state in the double-dot. This result is valid for $U > |\mu_1 \pm \mu_2| > J > k_BT, 2\pi\nu\Gamma^2$, with U the single-dot charging energy, ν the lead density of states, and Γ the tunneling amplitude between dots and leads. When calculating the zero-frequency noise [33] $S(\omega = 0)$ we find that the noise assumes its Poissonian value, $S(0) = -e|I|$ and no new information is gained. Moreover, when we calculate the finite frequency noise, $S(\omega)$, we no longer find a Poissonian behavior, but still we have $S(\omega) \propto (2 \pm \cos\varphi)$. Thus, *the current and noise reveal via the sign of the AB oscillations whether the double-dot is in a singlet or triplet state*. The triplets can be further distinguished by applying spatially inhomogeneous magnetic fields leading to a beating of the AB phase oscillation due to the Berry phase [33].

6.5. *Spin-dependent Josephson current through double dots [26]*

Finally we discuss a scenario, S-DD-S, with a double dot each dot of which is tunnel-coupled to superconducting leads [26]. These superconductors not only induce spin correlations between the two spins on the dots but also allow us to detect these correlations via the supercurrent traversing the dots. In particular, it turns out that this connection via a superconductor induces a Heisenberg exchange coupling between the two spins on the double dot, with an effective Hamiltonian,

$$H_{\text{eff}} \approx J(1+\cos\,\phi)\,\left[\mathbf{S}_a\cdot\mathbf{S}_{\text{b}}-\tfrac{1}{4}\right], \tag{13}$$

with $J \approx 2\Gamma^2/\epsilon$, where again Γ is the tunneling amplitude (between dot and lead), and ϵ the energy level of the dots below the lead Fermi level. Here, ϕ is the phase difference across the S-DD-S Josephson junction. Again, we see that we can tune the exchange coupling between the spins by tuning an external control parameter such as Γ or the phase ϕ. Connecting the superconducting leads into a SQUID-ring with one additional ordinary Josephson junction (of coupling J' and phase difference θ) and one S-DD-S junction we can drive a supercurrent I_{S} through the SQUID which will allow us to probe the spin states on the dots. Indeed, we find [26]

$$I_{\text{S}}/I_J = \begin{cases} \sin(\theta-2\pi f)+\alpha\,\sin\,\theta & \text{(singlet)},\\ \alpha\,\sin\,\theta & \text{(triplets)}, \end{cases} \tag{14}$$

where $I_J = 2eJ/\hbar$. When the system is biased by a dc current I larger than the spin- and flux-dependent critical current, given by $\max_\theta\{|I_{\text{S}}|\}$, a finite voltage V appears which then also depends on the spin states and thus allows one to *probe* the entanglement of the spins [26].

7. Conclusions

We have shown that the use of spin as qubit in electronic nanostructures offers a promising route toward the implementation of quantum gates, entangled states and quantum communication, with the possibility of upscaling that will eventually lead to quantum computers. The field of spintronics – the manipulation and detection of phase-coherent electron spins in the solid state – is a rapidly growing field of its own interest, and it is a fortunate situation that the study of quantum spin effects has promising applications not only for quantum computing and quantum communication but also for ordinary computer hardware (such as nonvolatile memories). We have discussed theoretical proposals how spins (qubits) can be manipulated via their charge degrees of freedom to achieve single-qubit and two-qubit gate operations, and how they can be transported in entangled EPR states which are needed for Bell measurements and eventually for quantum communication purposes.

References

1. Shor P.W., 1994. In: Proc. 35th Symposium on the Foundations of Computer Science (IEEE Computer Society Press), p. 124.
2. Grover L.K., 1997. Phys. Rev. Lett. 79, 325.
3. DiVincenzo D.P. and Loss D., 1999. J. Mag. Magn. Matl. 200, 202; cond-mat/9901137.
4. DiVincenzo D.P., Burkard G., Loss D. and Sukhorukov E., 1999. In: Kulik I.O. and Ellialtoglu R. eds. Quantum Mesoscopic Phenomena and Mesoscopic Devices in Microelectronics, NATO ASI Vol. C559, p. 399, Turkey, June 13–25; see cond-mat/99112445.
5. Shor P.W., 1995. Phys. Rev. A 52, 2493; Steane A.M., 1996. Phys. Rev. Lett. 77, 793; DiVincenzo D.P. and Shor P.W., 1996. Phys. Rev. Lett. 77, 3260.
6. Cirac J.I. and Zoller P., 1995. Phys. Rev. Lett. 74, 4091; Monroe C. et al., *ibid.* 75, 4714.
7. Turchette Q.A. et al., 1995. Phys. Rev. Lett. 75, 4710.
8. Cory D., Fahmy A. and Havel T., 1997. Proc. Nat. Acad. Sci. USA 94, 1634; Gershenfeld N.A. and Chuang I.L., 1997. Science 275, 350.
9. Loss D. and DiVincenzo D.P., 1998. Phys. Rev. A 57, 120. cond-mat/9701055.
10. Shnirman A., Schön G. and Hermon Z., 1997. Phys. Rev. Lett. 79, 2371.
11. Averin D.V., 1998. Solid State Commun. 105, 659.
12. Kane B., 1998. Nature 393, 133.
13. Ioffe L.B. et al., 1999. Nature 398, 679.
14. Orlando T.P. et al., 1999. Phys. Rev. B 60, 15 398.
15. Jacak L., Hawrylak P. and Wójs A., 1997. Quantum Dots, Springer, Berlin.
16. Tarucha S. et al., 1996. Phys. Rev. Lett. 77, 3613.
17. Kouwenhoven L.P. et al., 1997. In: Sohn L.L., Kouwenhoven L.P. and Schön G. eds. Proceedings of the ASI on Mesoscopic Electron Transport, Kluwer.
18. Waugh F.R. et al., 1995. Phys. Rev. Lett. 75, 705; Livermore, C. et al., 1996. Science 274, 1332.
19. Oosterkamp T.H. et al., 1998. Phys. Rev. Lett. 80, 4951.
20. Blick R.H. et al., 1998. Phys. Rev. Lett. 80, 4032; *ibid.* 81, 689; Oosterkamp T.H. et al., 1998. Nature 395, 873.

21. Kikkawa J.M., Smorchkova I.P., Samarth N. and Awschalom D.D., 1997. Science 277, 1284; Kikkawa J.M. and Awschalom D.D., 1998. Phys. Rev. Lett. 80, 4313; Awschalom D.D. and Kikkawa J.M., 1999. Phys. Today 52, 33.
22. Gupta J.A., Awschalom D.D., Peng X. and Alivisatos A.P., 1999. Phys. Rev. B 59, R10421.
23. Barenco A. et al., 1995. Phys. Rev. A 52, 3457.
24. Burkard G., Loss D. and DiVincenzo D.P., 1999. Phys. Rev. B 59, 2070.
25. Imamoglu A., Awschalom D.D., Burkard G., DiVincenzo D.P., Loss D., Sherwin M. and Small A., 1999. Phys. Rev. Lett. 83, 4204.
26. Choi M.-S., Bruder C. and Loss D. to appear in Phys. Rev. B., cond-mat/0001011.
27. Luyken R.J. et al., preprint.
28. Austing D.G. et al., 1998. Physica B 249–251, 206.
29. Burkard G., Seelig G. and Loss D., 2000. Phys. Rev. B 62, 2581.
30. Ivchenko E.L., Kiselev A.A. and Willander M., 1997. Solid State Comm. 102, 375.
31. Kiselev A.A., Ivchenko E.L. and Rössler U., 1998. Phys. Rev. B 58, 16 353.
32. Burkard G., Loss D. and Sukhorukov E.V., 2000, Phys. Rev. B 61, R16303.
33. Loss D. and Sukhorukov E.V., 2000. Phys. Rev. Lett. 84, 1035; cond-mat/9907129.
34. Bennett C.H. and Brassard G., 1984. In: Proceedings of the IEEE International Conference on Computers, Systems and Signal Processing, Bangalore, India, IEEE, NY, p. 175.
35. Einstein A., Podolsky B. and Rosen N. 1935. Phys. Rev. 47, 777.
36. Aspect A., Dalibard J. and Roger G., 1982. Phys. Rev. Lett. 49, 1804; Tittel W. et al., 1998. Phys. Rev. Lett. 81, 3563.
37. Boumeester D. et al., 1997. Nature 390, 575; Boschi D. et al., 1998. Phys. Rev. Lett. 80, 1121.
38. Loudon R., 1990. In: Eberly J.H. et al., eds. Coherence and Quantum Optics VI, Plenum, New York.
39. Hanbury Brown R. and Twiss R.Q., 1956. Nature (London) 177, 27.
40. Büttiker M., 1990. Phys. Rev. Lett. 65, 2901; Phys. Rev. B 46, 12 485 (1992).
41. Martin T. and Landauer R., 1992. Phys. Rev. B 45, 1742.
42. Liu R.C., Odom B., Yamamoto Y. and Tarucha S., 1998. Nature 391, 263; Henny M., Oberholzer S., Strunk C., Heinzel T., Ensslin K., Holland M. and Schönenberger C., 1999. Science 284, 296; Oliver W.D. et al., 1999. Science 284, 299.
43. Prinz G.A., 1998. Science 282, 1660.
44. Khlus V.A., 1987. Zh. Eksp. Teor. Fiz. 93, 2179.
45. Loss D., Burkard G. and Sukhorukov E.V., 1999. In: Proceedings of the XXXIVth Recontres de Moriond 'Quantum Physics at the Mesoscopic Scale', Les Arcs, Savoie, France, January 23–30.
46. Sukhorukov E. and Loss D., 1999. In: Kulik I.O. ed. Quantum Mesoscopic Phenomena and Mesoscopic Devices in Microelectronics, NATO Advanced Study Institute Vol. C559, p. 243, Turkey, June 13–25.